ISSN 0915-633X

NATIONAL INSTITUTE FOR FUSION SCIENCE

Development of a High-Current Hydrogen-Negative Ion Source for LHD-NBI System

Y. Takeiri, M. Osakabe, K. Tsumori, Y. Oka, O. Kaneko, E. Asano, T. Kawamoto, R. Akiyama and M. Tanaka

(Received - Aug. 6, 1998)

NIFS-557 Aug. 1998

RESEARCH REPORT
NIFS Series

NAGOYA, JAPAN

Development of a High-Current Hydrogen-Negative Ion Source for LHD-NBI System

TAKEIRI Yasuhiko, OSAKABE Masaki, TSUMORI Katsuyoshi, OKA Yoshihide,
KANEKO Osamu, ASANO Eiji, KAWAMOTO Toshikazu, and AKIYAMA Ryuichi
National Institute for Fusion Science, Toki, Gifu 509-5292, Japan
TANAKA Masanobu
Power and Industrial Systems R&D Division, Hitachi, Ltd., Ibaraki 316, Japan

Abstract

We have developed a high-current hydrogen-negative ion source for a negative-ion-based NBI system in Large Helical Device (LHD). The ion source is a cesium-seeded volume-production source equipped with an external magnetic filter. An arc chamber is rectangular, the dimensions of which are 35 cm x 145 cm in cross section and 21 cm in depth. A three-grid single-stage accelerator is divided into five sections longitudinally, each of which has 154 (14 x 11) apertures in an area of 25 cm x 25 cm. The ion source was tested in the negative-NBI teststand, and 25 A of the negative ion beam is incident on a beamdump 13 m downstream with an energy of 104 keV for 1 sec. Multibeamlets of 770 are focused on a focal point 13 m downstream with an averaged divergence angle of 10 mrad by the geometrical arrangement of five sections of grid and the aperture displacement technique of the grounded grid. A uniform beam in the vertical direction over 125 cm is obtained with uniform plasma production in the arc chamber by balancing individual arc currents flowing through each filament. Long-pulse beam production was performed, and 1.3 MW of the negative ion beam is incident on the beamdump for 10 sec, and the temperature rise of the cooling water is almost saturated for the extraction and the grounded grids. These results satisfy the first-step specification of the LHD-NBI system.

Keywords : NBI system, negative ion source, Large Helical Device, cesium-seeded volume production, external magnetic filter, aperture displacement technique, long-pulse beam production

1. Introduction

Large Helical Device (LHD) is the world-largest superconducting helical device with a major radius of 3.9 m [1,2], and started its operation at the end of March in 1998 [3]. Neutral beam injection (NBI) heating system in LHD is a main heating device for achievement of the target plasma parameters in LHD, and was projected to use negative ion beams because the required injection energy is more than 100 keV for hydrogen where the neutralization efficiency of positive ions is extremely low, less than 20 % [4]. From the detailed design study on the negative-ion-based LHD-NBI system, the injection energy and power were determined at 180 keV for hydrogen and 15 MW, respectively, using two injectors arranged tangentially and balanced [5].

In the LHD-NBI system an injector has two negative ion sources, each of which has to produce 180 keV - 40 A negative ion beams to satisfy the specification. We adopted the two-step development of the LHD-NBI negative ion source. In the first step a high-current negative ion source of 30 A should be developed with an energy of 100 - 180 keV, leading to 10 MW of the total injection power at maximum, for the first two - three years of LHD experiments. During this experimental period, the negative ion source should be up-graded to 180 keV - 40 A of the negative ion beam production as the second-step development.

We started the R&D of negative ion sources in 1990, with a volume-production multi-cusp bucket source using the rod magnetic filter [6]. By introducing cesium vapor into the arc chamber, a negative ion beam with a high current density of 54 mA/cm^2 was produced [7], and then 16 A of the negative ion current was obtained [8]. To improve the source efficiencies such as the arc efficiency and the operational gas pressure, the external magnetic filter was used, and 16.2 A of the negative ion beam was extracted at a high arc efficiency of 0.1 A/kW and at a low operational gas pressure of 3.8 mTorr [9]. A high-energy acceleration of 13.6 A of the negative ion beam was also achieved up to 125 keV [10]. Multibeamlets from a large area were successfully focused using the aperture displacement technique of the grounded grid and an averaged divergence angle of 9 mrad was achieved [11]. Accelerated electrons leading to heat load of the downstream grid were suppressed by shaping the beam aperture of the extraction grid [12]. As a result, a long-pulse negative ion beam was produced for 10 sec with a beam power of 330 kW [13].

Based on these R&D results, the LHD-NBI negative ion sources have been designed and constructed [14-16], in parallel to the injector construction [17,18]. The construction of two injectors (BL1 and BL2) has been sequential and, thus, the detailed design of ion sources in the BL1 and the BL2 is a little different to incorporate the advanced R&D results. The LHD-NBI sources for both the BL1 and the BL2 have been tested on the negative-ion-based NBI teststand [19-21], and the results have almost satisfied the first-step requirements of the LHD-NBI system. Here, we present the BL2 ion source results.

In this paper, we explain the detailed structure of the LHD-NBI source for the BL2 first. Next, the characteristics of the negative ion beams are presented with respect to the high-current negative ion production, the long-pulse operation, and the beam uniformity. The problems to be solved for the second-step requirements of the LHD-NBI system are also discussed.

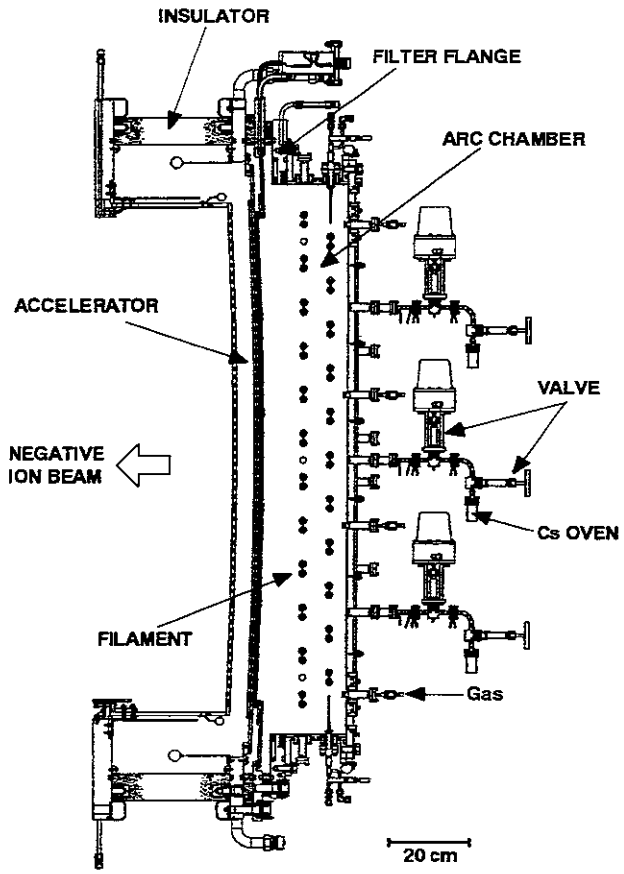

Fig. 1 Schematic diagram of a large hydrogen-negative ion source for the LHD-NBI system. The negative ion beam is extracted and accelerated toward the left hand side.

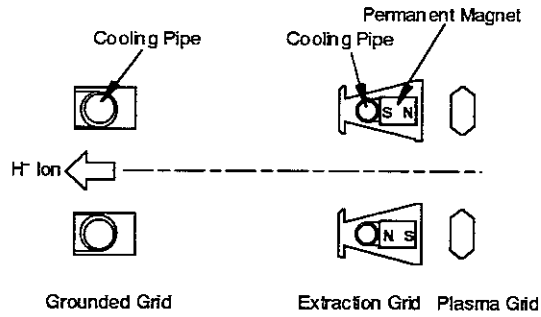

Fig. 2 Schematic diagram of a three-grid and single-stage negative ion accelerator, showing a cross section for one beamlet.

2. Structure of LHD-NBI Source

A schematic diagram of an LHD-NBI negative ion source is shown in Fig. 1. The ion source is a cesium-seeded volume-production source [22,23] equipped with external magnetic filter [24]. An arc chamber made of copper has dimensions of 35 cm x 145 cm in cross section and 21 cm in depth, which is surrounded by cusp magnetic field. The cusp magnetic field strength is around 2 kG on the inner chamber surface. The external magnetic filter is generated laterally in front of a plasma grid by a pair of permanent magnet rows facing each other with a separation of 35 cm. The permanent magnets are contained in a filter flange made of copper and water-cooled. The filter magnetic field is uniform in the longitudinal direction, and the magnetic field strength at the center is 52 G. Thick tungsten filaments of 1.8 mm in diameter are used for the arc discharge. Although the arc chamber is equipped with 48 filament feedthroughs, only 24 filaments are used, which are enough for the arc discharge of 200 kW. Three cesium ovens are attached to a back plate of the arc chamber, and are heated with their temperature controlled. The cesium vapor injection is remotely controlled with an air-actuated valve.

A negative ion accelerator is a three-grid and single-stage one, and consists of plasma grid, extraction grid, and grounded grid, as shown in Fig. 2. The grid area is 25 cm x 125 cm and is divided into five sections longitudinally, which are jointed with an angle of 19.2 mrad so that each section is aimed at a focal point 13 m downstream. The plasma grid (PG) is made of molybdenum and thermally insulated to keep the PG temperature above 200 ℃ for increasing in the negative ion current by the cesium effect [7,25,26]. A thermocouple is attached on each section for monitoring the PG temperature. There are 154 (14 x 11) apertures of 13 mm in diameter in one section of grid, and the transparency is 35 %. The extraction grid (EG) is made of copper. Between beam aperture rows, a water-cooling pipe is buried laterally for active cooling of the gird. In the same direction, a permanent magnet row is also buried for electron suppression, touching the water-cooling pipe, as shown in Fig. 2. The maximum magnetic field strength on the beam axis is around 500 G, and the extracted electrons would be deflected and be incident on the EG. The inside of the beam aperture is so shaped as the secondary electrons generated on the inner surface of the beam aperture would be prevented from entering the acceleration gap [12]. The narrower end aperture works as a shield against the acceleration electric field and reduces the electron leakage. The grounded grid (GG) is also made of copper and fully water-cooled by cooling pipes buried between aperture rows. The apertures of the GG are displaced so that all beamlets would be gathered on a focal point 13 m downstream. The magnetic field at the EG deflects also the negative ion beamlet laterally. Since the deflection direction alternates line by line longitudinally, the aperture displacement for the correction of this alternate beamlet deflection is superimposed line by line according to the deflection direction [11]. The amount of displacement is determined based on the 3-dimensional beam trajectory simulation [27]. The aperture displacement technique is applied to each section of grid individually, and all beamlets of 770 are focused on a focal point 13 m downstream with the geometrical arrangement of five sections of grid.

The extraction gap is adjustable of 5 - 7 mm, and the maximum applied voltage is 15 kV. The acceleration

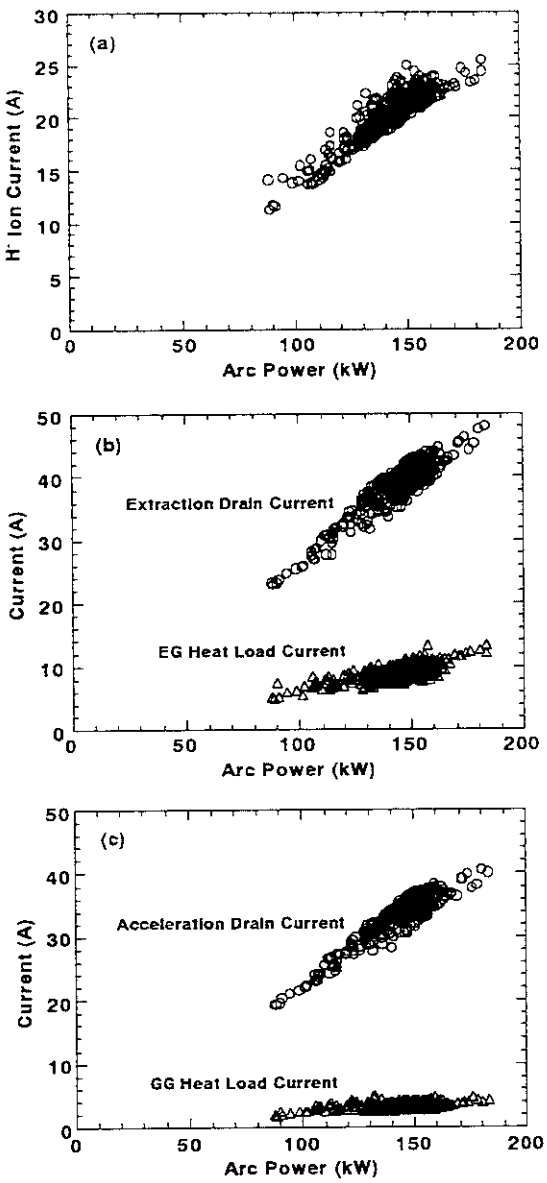

Fig. 3 (a) Negative ion current measured at the beamdump 13 m downstream, (b) the extraction drain current and the equivalent heat load current to the extraction grid, and (c) the acceleration drain current and the equivalent heat load current to the grounded grid, as a function of the arc power. The total beam energy is 68 - 105 keV and the operational gas pressure is 2.2 - 2.8 mTorr. The pulse length is 1.0 sec.

gap is 34 mm or 46 mm depending on a target beam energy of 120 keV or 180 keV, respectively. Since the target beam energy is 120 keV at the initial injection into LHD, the acceleration gap was adjusted at 34 mm in the full-grid area experiments. A thick insulator for high-voltage holding and vacuum seal is made of voidless FRP (fiber resin plastic).

The ion source is installed to the negative-ion-based NBI teststand [19-21]. At first, only a central section of grid is used and the other sections are masked (1/5-grid area experiments). After that the negative ion beams are produced from all five sections of gird (full-grid area experiments). Two cross-shaped movable calorimeter arrays 4.2 m and 10.4 m downstream are used for the negative ion detection and the profile measurement in the 1/5-grid area experiments. In the full-grid area experiments, only the calorimeter array 10.4 m downstream is used for the profile measurement at a low negative ion beam power. At a high negative ion beam power, the negative ion current is estimated with water-calorimetry of a beam-dump 13 m downstream. Heat loads of the EG and the GG are measured also with the water-calorimetry. The equivalent heat load currents to the EG and the GG are estimated by dividing the heat load by both the pulse length and the applied voltage to the upstream gap.

The pulse length is 0.6 - 1.0 sec except for long-pulse experiments.

3. Characteristics of Negative Ion Beam

3.1 High-current negative-ion beam production

In the full-grid area experiments, a high-current negative ion beam was obtained. Figure 3 (a) shows the negative ion current measured at the beamdump 13 m downstream as a function of the arc power. The negative ion current is proportional to the 3/2-power of the total beam energy [10], and the extraction and the acceleration voltages are changed with a constant ratio. In Fig. 3 (a), the total beam energy is changed 68 - 105 keV according to the negative ion current, and the operational gas pressure is 2.2 - 2.8 mTorr. The pulse length is 1.0 sec. The negative ion current is proportional to the arc power and reaches 25 A with an energy of 104 keV. The arc efficiency, defined as the negative ion current divided by the arc power, is as high as 0.14 A/kW. The extraction drain current and the equivalent heat load current to the EG are shown in Fig. 3 (b), as a function of the arc power. The negative ion current 13 m downstream is about 53 % of the extraction current, and the heat load current to the EG is about 27 % of the extraction current. It is found that the extracted electron current is much suppressed and the heat load of the EG is small. Figure 3 (c) shows the acceleration drain current and the equivalent heat load current to the GG as a function of the arc power. The acceleration efficiency, defined as a ratio of the negative ion current to the acceleration current, is about 62 %, and the heat load current to the GG is about 10 % of the acceleration current. The acceleration efficiency is relatively low compared with the R&D results, while the GG heat load ratio is not so high [12]. The negative ion transmission loss through the neutralizer would cause the lower acceleration efficiency, although an increase in accelerated electrons which leak out of the EG could be an another cause.

3.2 Gas pressure dependence

Low gas pressure operation is quite important for negative ion sources for reduction of the stripping loss of negative ions during the acceleration. Figure 4 shows the negative ion current measured 4.2 m downstream, the acceleration efficiency and the equivalent heat load current to the GG as a function of the operational gas pressure in

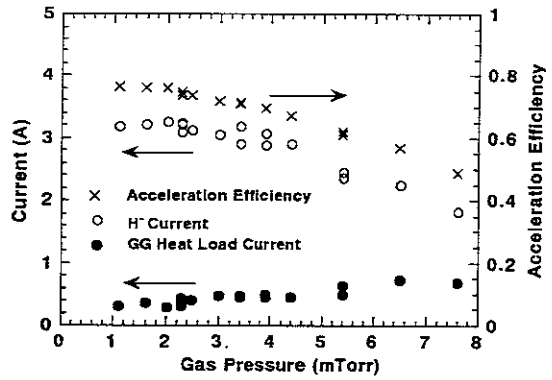

Fig. 4 Negative ion current measured 4.2 m downstream, the acceleration efficiency, and the equivalent heat load current to the grounded grid as a function of the operational gas pressure in the 1/5-grid area experiments. The arc power is 100 kW.

the 1/5-grid area experiments. The arc power is 100 kW. As shown in Fig. 4, the negative ion current does not deteriorate even at a low gas pressure of 1 mTorr. The GG heat load current is decreased with a decrease in the gas pressure due to the reduction of the stripped electrons during the negative ion acceleration. Although the acceleration efficiency is increased with a decrease in the gas pressure, it is not extrapolated to 100 % at a gas pressure of 0, meaning that the electron leakage into the acceleration gap from the extraction grid is not fully suppressed. The optimum operational gas pressure tends to increase with increasing the arc power, and at above 150 kW a gas pressure of 2.5 - 3.0 mTorr is required for an efficient negative ion production.

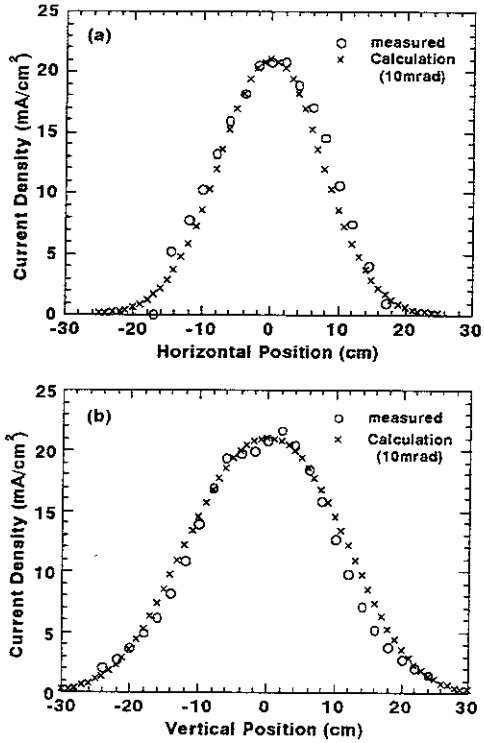

Fig. 5 (a) Horizontal and (b) the vertical beam profiles measured at the calorimeter array 10.4 m downstream in the full-grid area experiments. The arc power is 90 kW and the beam energy is 68 keV. The estimated negative ion current from these profiles is 11.0 A. The calculated profiles are also indicated using multi-gaussian beamlets of 770 with a divergence angle of 10 mrad and a focal length of 13 m.

3.3 Beam profile

The beam divergence angle is required to be less than 10 mrad for the LHD-NBI system, where the injection port diameter is 52 cm. The beam profile is measured both horizontally and vertically with the calorimeter array 10.4 m downstream from the ion source in the full-grid area experiments. Figures 5 (a) and (b) show the horizontal and the vertical profiles, respectively, with a relatively small arc power of 90 kW due to the calorimeter protection. The beam energy is 68 keV and the detected negative ion current at the calorimeter is 11.0 A. The calculated profiles are also indicated in the figures with multi-gaussian beamlets of 770, each of which has a divergence angle of 10 mrad and a focal length of 13 m. It is found that the measured profiles are well fitted to the calculated ones and is considered that the averaged divergence angle is around 10 mrad. In the horizontal profile, the measured one is a little broader than the calculated one. The negative ion beam is deflected horizontally by the magnetic field at the extraction grid, the deflection direction of which is alternate line by line in the vertical direction, as explained in section 2. Although the aperture displacement of the grounded grid compensates this deflection electrostatically, there remains the alternate deflection because of an under-compensation due to the lower extraction and acceleration voltages. On the other hand, in the vertical profile the measured profile is a little narrower than the calculated one. Beam uniformity in the vertical direction would be a little lowered at the top or bottom ends, which is discussed in section 3.5.

3.4 Long-pulse beam production

Steady-state NBI experiments are proposed in LHD [28]. The long-pulse negative-ion beam production was tested for 10 sec, which is the maximum pulse length in the teststand. Figure 6 (a) shows the beamdump heat load as a function of the pulse duration. The beam energy is 81 keV, the arc power is 110 kW, and the operational gas pressure is 1.9 mTorr. The beamdump heat load is proportional to the pulse duration, and it is found that 1.3 MW of the negative ion beam is incident on the beamdump 13 m downstream for 10 sec. The negative ion current and the equivalent heat load currents to the EG and the GG are shown in Fig. 6 (b), as a function of the pulse duration. No change of these heat load currents is observed for 10 sec, meaning that the negative ion beam properties are almost constant for 10 sec. Figure 7 shows the temporal behaviors of the extraction voltage and cur-

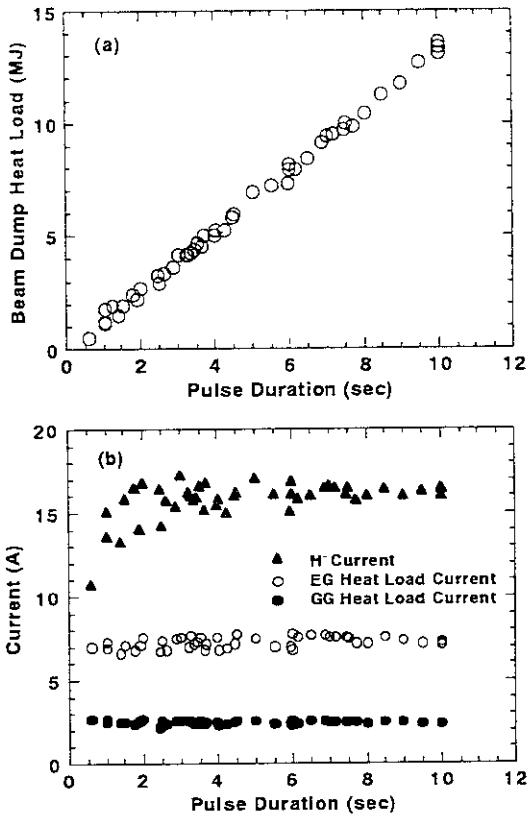

Fig. 6 (a) Beam dump heat load, and (b) the negative ion current and the equivalent heat load currents to the extraction grid and the grounded grid, as a function of the pulse duration. The beam energy is 81 keV, the arc power is 110 kW, and the operational gas pressure is 1.9 mTorr.

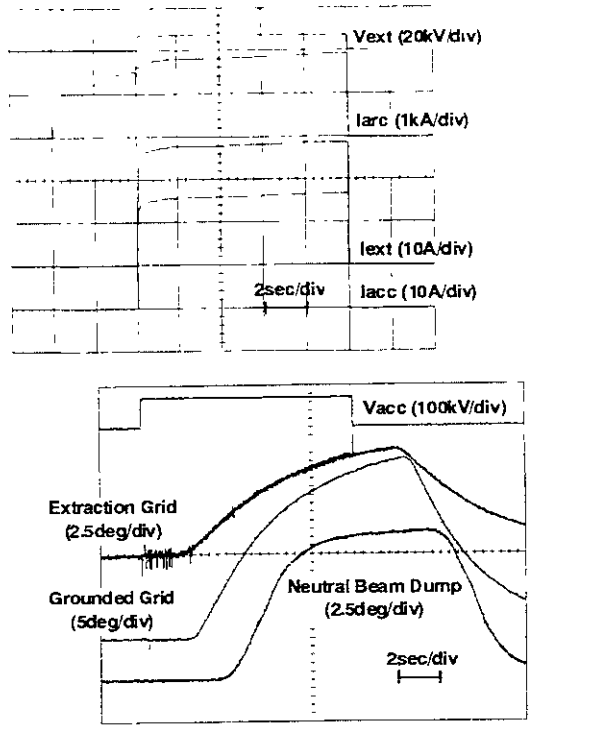

Fig. 7 Temporal behaviors of the extraction voltage and current, the acceleration voltage and current, the arc current, and the temperature rises of cooling water of the extraction gird, the grounded grid and the beamdump in a long-pulse operation of 10 sec. The negative ion energy is 81 keV and the beam power at the beamdump is 1.3 MW.

rent, the acceleration voltage and current, the arc current, and the temperature rises of cooling water of the extraction grid, the acceleration grid and the beamdump for a 10 sec-beam pulse of 1.3 MW. Although the temperature rises of the EG and the GG do not reach a steady state in 10 sec, they are 6 ℃ and 21 ℃, respectively, and tend to saturate. Therefore, a steady-state operation in this power level is possible. The temperature rise of the beamdump made of swirl tube saturates quickly.

3.5 Uniformity

Since the ion source is vertically long and horizontally narrow, uniformity of the negative ion beam intensity in the vertical direction is important. That should be mainly determined by plasma uniformity in the arc chamber. In the negative ion source, the strong filter magnetic field, which is transverse in the narrow direction, is employed for the negative ion production, together with the strong cusp magnetic field for the efficient plasma confinement. To produce the uniform plasma in this magnetized arc chamber, individual arc currents flowing through each filament are controlled with variable resistances inserted between the twelve outputs of the arc power supply and twelve electrically isolated filament power supplies [13]. The time variation of individual arc currents are shown in Figs. 8 (a) and (b). The total arc current is 2000 A. 24 filaments are arranged on both sidewalls symmetrically, and Figs. 8 (a) and (b) show 12 individual arc currents on the left and the right hand sides, respectively. As shown in the figures, after about 4 sec from the plasma initiation the individual arc currents are steady and almost the same within ± 10 % except for two bottom filaments. Horizontal uniformity (symmetry) is high. Since the individual arc current distribution reflects the plasma uniformity [16], the produced plasma with the high-arc power is considered to be uniform although in the bottom area the plasma density would be a little lower. This uniform and steady plasma production is important for long-pulse negative ion beam production [13].

The plasma grid temperatures of five sections are measured. Although the temperatures of the top and bottom sections are lower than those of the central three sections by 30 - 50 ℃, the temperatures of all sections range from 200 to 300 ℃ for various arc powers, that satisfies the efficient negative ion production condition in the cesium-seeded mode.

The heat loads of the extraction and the grounded grid are measured for five sections. Figures 9 (a) and (b) shows the EG and the GG heat loads, respectively, of the

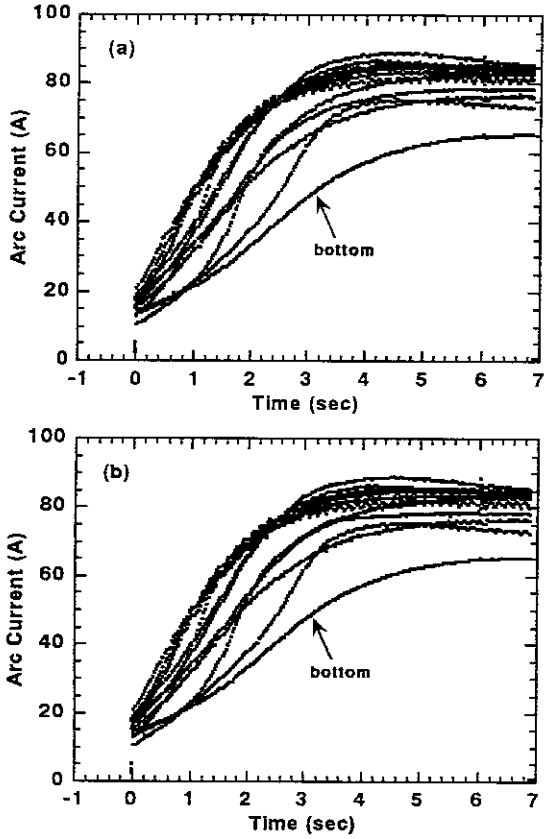

Fig. 8 Time variation of individual arc currents flowing through each filament (a) on the left hand side and (b) on the right hand side. The total arc current is 2000 A.

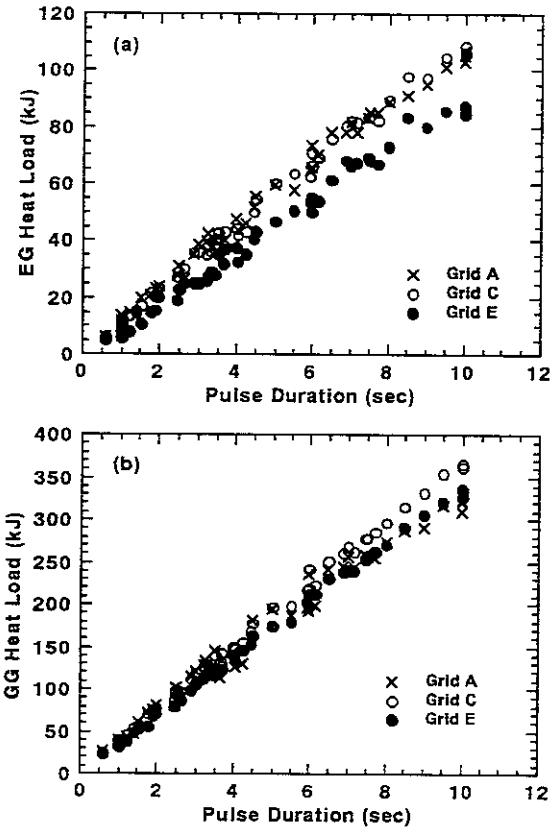

Fig. 9 Heat loads measured on the top, the center, and the bottom sections (a) in the extraction grid and (b) in the grounded grid, as a function of the pulse duration. The experimental conditions are the same as those in Fig. 6.

top, center and bottom sections in the long-pulse operation in Fig. 6. The heat load of bottom section in the EG is a little lower than that of the other sections, corresponding to the individual arc current distribution in Fig. 8. The EG heat load is ascribed to the extracted electron current, which is related with the plasma density near the plasma grid. Since the cesium distribution and the PG temperature distribution are almost uniform in the vertical direction, the lower EG heat load is thought to be related with lower negative ion current resulting from the lower plasma density. On the other hand, the GG heat load is uniform. The beam trajectory of the bottom section should be worse due to the lower negative ion current, and, therefore, the heat load ratio would be increased, resulting in the nearly same heat load as those in the other sections.

The beam uniformity is considered to be high, judging from the plasma uniformity and the uniformity of the grid heat load. In the bottom area, however, the negative ion beam intensity seems to be a little lower, that would result in the narrower vertical beam profile as shown in Fig. 5 (b).

4. Discussion and Future Prospective

The LHD-NBI source produces a negative ion beam of 25 A, which is detected at the beamdump 13 m downstream. This value is now the world highest negative ion current. Assuming a transmission efficiency of the 5 m-neutralizer at about 90 %, the negative ion current before entering the neutralizer is estimated at about 28 A. If the acceleration efficiency before entering the neutralizer is 75 %, which is the same as that in the 1/5-grid area experiments, the negative ion current is about 30 A from Fig. 3 (c). Therefore, it is thought that the first-step goal has been achieved for the negative ion current. A low operational gas pressure of below 3 mTorr, a high arc efficiency of 0.14 A/kW, and a small averaged divergence angle of 10 mrad also satisfy the LHD-NBI source requirements.

However, there are some problems to be solved for the second-step goal of 40 A of the negative ion beam production. Improvement of the acceleration efficiency is the most important issue. In the LHD-NBI source specification, 89 % of the acceleration efficiency is required before entering the neutralizer. By strengthening the magnetic field at the extraction grid and optimizing the aperture shape of the extraction grid, the acceleration efficiency could be improved due to reduction of the electron leakage into the acceleration gap. Lowering the operational gas pressure is also important to improve the acceleration efficiency because of reduction of the stripped

electrons during the negative ion acceleration. Improvement of the arc plasma confinement by strengthening the cusp magnetic field could be effective to lower the gas pressure. The improvement of the acceleration efficiency would result in reduction of the GG heat load, leading to a high-power steady-state operation of the ion source.

An another trend to the negative ion source development is to produce deuterium negative ions for D-D experiments planned in the second-phase LHD.

5. Concluding Remarks

We have developed a large hydrogen-negative ion source for the LHD-NBI system, which is equipped with two beamlines (BL1 and BL2) arranged as tangential and balanced injection. Each beamline has two ion sources, and the characteristics of BL2 ion sources (IS2A and IS2B) are presented here. In the negative-ion-based NBI teststand, 25 A of the negative ion beam is incident on the beamdump 13 m downstream through the neutralizer with an energy of 104 keV. The operational gas pressure is as low as 2.8 mTorr, and the averaged beam divergence angle is around 10 mrad. The beam uniformity is high in the vertical direction over 125 cm. These results satisfy the first-step specification for the LHD-NBI source. There are problems to be solved for the second-step specification. The improvement of the acceleration efficiency is necessary for the further increase in the negative ion current and the reduction of the heat load of the grounded grid. Long-pulse production of a negative ion beam of 1.3 MW is achieved for 10 sec, where the temperature rises of cooling water of the extraction and the grounded grids are almost saturated. This result enables steady-state neutral beam injection of above 1 MW for 30 min, which is projected in LHD [28].

Two ion sources of IS2A and IS2B show almost the same properties such as the achieved negative ion current, the operational gas pressure, the arc efficiency, and the averaged beam divergence angle. The first injection into the LHD plasma is scheduled in September, 1998, and the injector properties of the negative-ion based LHD-NBI system and the NBI-heated LHD plasma properties will be presented elsewhere.

Acknowledgements

The authors would like to greatly acknowledge Professor A. Iiyoshi, Director-General, for his continuous encouragement and support to the development of the ion source. They also wish to express their gratitude to Professors M. Fujiwara, O. Motojima, and T. Watari for their encouragement and support.

References

[1] A. Iiyoshi, M. Fujiwara, O. Motojima, N. Ohyabu and K. Yamazaki, Fusion Technology **17**, 169 (1990).

[2] O. Motojima, K. Akaishi, M. Asao, K. Fujii, J. Fujita, *et al.*, *Proc. of the 13th IAEA Conference on Plasma Physics and Controlled Nuclear Fusion Research (Washington, 1990)* Vol. 3, p. 513.

[3] A. Iiyoshi, to be presented in *the 17th IAEA Fusion Energy Conference (Yokohama, Japan, 1998)*, OV1/4.

[4] Y Takeiri, O. Kaneko, F. Sano, A Ando, Y. Oka, K. Hanatani, T Obiki and T. Kuroda, *Proc. of the first Int. Toki Conf. on Plasma Physics and Controlled Nuclear Fusion (Toki, Japan, 1989)*, p. 272.

[5] O. Kaneko, Y. Takeiri, K. Tsumori, Y. Oka, M. Osakabe, R. Akiyama, T. Kawamoto, E. Asano, and T. Kuroda, *Proc. of the 16th IAEA Fusion Energy Conference (Montreal, Canada, 1996)* Vol. 3, p. 539.

[6] Y. Takeiri, A. Ando, O. Kaneko, Y. Oka, R. Akiyama, T. Kawamoto, A. Karita, K. Mineo and T. Kuroda, *Proc. of the 16th Symp. on Fusion Technology (London, 1990)*, p. 1012.

[7] A. Ando, K. Tsumori, Y. Takeiri, O. Kaneko, Y. Oka, T. Okuyama, H. Kojima, Y. Yamashita, R. Akiyama, T. Kawamoto, K. Mineo, T. Kurata and T. Kuroda, *Proc. of the 6th Int. Symp. on Production and Neutralization of Negative Ions and Beams (Upton, NY, 1992)*, AIP Conf. Proc. No. 287, p. 339.

[8] A. Ando, K. Tsumori, Y. Oka, O. Kaneko, Y. Takeiri, E. Asano, T. Kawamoto, R. Akiyama and T. Kuroda, Phys. Plasmas **1**, 2813 (1994).

[9] Y. Takeiri, A. Ando, O. Kaneko, Y. Oka, K. Tsumori, R. Akiyama, E. Asano, T. Kawamoto, T. Kuroda, M. Tanaka and H. Kawakami, Rev. Sci. Instrum. **66**, 2541 (1995).

[10] Y. Takeiri, A. Ando, O. Kaneko, Y. Oka, K. Tsumori, R. Akiyama, E. Asano, T. Kawamoto, M. Tanaka and T. Kuroda, J. Plasma Fusion Res. **71**, 605 (1995).

[11] Y. Takeiri, O. Kaneko, Y. Oka, K. Tsumori, E. Asano, R. Akiyama, T. Kawamoto, T. Kuroda, and A. Ando, Rev. Sci. Instrum. **66**, 5236 (1995).

[12] Y. Takeiri, Y. Oka, M. Osakabe, K. Tsumori, O. Kaneko, T. Takanashi, E. Asano, T. Kawamoto, R. Akiyama, and T. Kuroda, Rev. Sci. Instrum. **68**, 2003 (1997).

[13] Y. Takeiri, M. Osakabe, Y. Oka, K. Tsumori, O. Kaneko, T. Takanashi, E. Asano, T. Kawamoto, R. Akiyama, and T. Kuroda, Rev. Sci. Instrum. **68**, 2012 (1997).

[14] Y. Takeiri, M. Osakabe, K. Tsumori, Y. Oka, O. Kaneko, E. Asano, T. Kawamoto, and R. Akiyama, Rev. Sci. Instrum. **69**, 977 (1998).

[15] Y. Oka, K. Tsumori, Y. Takeiri, O. Kaneko, M. Osakabe, E. Asano, T. Kawamoto, and R. Akiyama, Rev. Sci. Instrum. **69**, 920 (1998).

[16] K. Tsumoi, M. Osakabe, Y. Takeiri, O. Kaneko, Y. Oka, E. Asano, O. Kaneko, S. Asano, T. Okuyama, Y. Suzuki, and T. Takanashi, *Proc. of the Joint Meeting of the 8th Int. Symp. on Production and Neutralization of Negative Ions and Beams and the 7th European Workshop on the Production and Application of Light Negative Ions (Villagium of Giens, France, 1997),* to be published.

[17] O. Kaneko, Y. Oka, M. Osakabe, Y. Takeiri, K. Tsumori, R. Akiyama, E. Asano, T. Kawamoto, A. Ando, and T. Kuroda, *Proc. of the 16th IEEE/NPSS Symp. on Fusion Engineering (Champaign, 1995)* Vol. 2, p. 1082.

[18] Y. Takeiri, O. Kaneko, Y. Oka, K. Tsumori, M Osakabe, R. Akiyama, T. Kawamoto, E. Asano, *Proc. of the 17th IEEE/NPSS Symp. on Fusion Engineering (San Diego, 1997)* Vol. 1, p. 409.

[19] Y. Oka, A. Ando, O. Kaneko, Y. Takeiri, K. Tsumori, R. Akiyama, T. Kawamoto, K. Mineo, T. Kurata and T. Kuroda, *Proc. of the 14th IEEE/NPSS Symp. on Fusion Engineering (San Diego, 1991)* Vol. 1, p. 70.

[20] O. Kaneko, A. Ando, Y. Oka, Y. Takeiri, K. Tsumori, R. Akiyama, T. Kawamoto, T. Kurata, K. Mineo and T. Kuroda, *Proc. of the 17th Symp.on Fusion Technology (Rome,*

1992), p. 544.

[21] Y. Takeiri, A. Ando, O. Kaneko, Y. Oka, K. Tsumori, R. Akiyama, T. Kawamoto and T. Kuroda, *Proc. of the 6th Int. Symp. on Production and Neutralization of Negative Ions and Beams, Upton, NY, 1992*, AIP Conf. Proc. No. 287, p. 869.

[22] S. R. Walther, K. N. Leung and W. B. Kunkel, J. Appl. Phys. **64**, 3424 (1988).

[23] Y. Okumura, M. Hanada, T. Inoue, H. Kojima, Y. Matsuda, Y. Ohara, Y. Oohara, M. Seki, Y. Suzuki and K. Watanabe, *Proc. of the 16th Symp. on Fusion Technology (London, 1990)*, p. 1026.

[24] G. Dammertz and B. Piosczyk, *Proc. of the 4th Int. Symp. on Heating in Troidal Plasmas (Rome, 1984)* Vol. 2, p. 1087.

[25] Y. Okumura, M. Hanada, T. Inoue, H. Kojima, Y. Matsuda, Y. Ohara, M. Seki and K. Watanabe, *Proc. of the 5th Int. Symp. on the Production and Neutralization of Negative Ions and Beams (Brookhaven, 1990)*, AIP Conf. Proc. No. 210, p. 169.

[26] T. Inoue, M. Hanada, M. Mizuno, Y. Ohara, Y. Okumura, Y. Suzuki, M. Tanaka and K. Watanabe, *Proc. of the 6th Int. Symp. on Production and Neutralization of Negative Ions and Beams (Upton, NY, 1992)*, AIP Conf. Proc. No. 287, p. 316.

[27] M. Tanaka, Y. Ose, M. Koizumi, Y. Yamashita, H. Kawakami, Y. Takeiri, O. Kaneko, Y. Oka, K. Tsumori, and M. Osakabe, Rev. Sci. Instrum. **69**, 1144 (1998).

[28] Y. Takeiri, O. Kaneko, Y. Oka, K. Tsumori, M. Osakabe, R. Akiyama, T. Kawamoto, and E. Asano, J. Plasma and Fusion Res. SERIES **1**, 405 (1998).

Recent Issues of NIFS Series

NIFS-521 K. Ida, S Nishimura, T Minami, K Tanaka, S Okamura, M. Osakabe, H Idei, S Kubo, C Takahashi and K Matsuoka,
High Ion Temperature Mode in CHS Heliotron/torsatron Plasmas; Nov 1997

NIFS-522 M. Yokoyama, N Nakajima and M Okamoto,
Realization and Classification of Symmetric Stellarator Configurations through Plasma Boundary Modulations; Dec. 1997

NIFS-523 H Kitauchi,
Topological Structure of Magnetic Flux Lines Generated by Thermal Convection in a Rotating Spherical Shell; Dec 1997

NIFS-524 T. Ohkawa,
Tunneling Electron Trap; Dec 1997

NIFS-525 K Itoh, S.-I Itoh, M. Yagi, A Fukuyama,
Solitary Radial Electric Field Structure in Tokamak Plasmas, Dec. 1997

NIFS-526 Andrey N Lyakhov,
Alfven Instabilities in FRC Plasma, Dec. 1997

NIFS-527 J. Uramoto,
Net Current Increment of negative Muonlike Particle Produced by the Electron and Positive Ion Bunch-method; Dec 1997

NIFS-528 Andrey N Lyakhov,
Comments on Electrostastic Drift Instabilities in Field Reversed Configuraiton, Dec. 1997

NIFS-529 J. Uramoto,
Pair Creation of Negative and Positive Pionlike (Muonlike) Particle by Interaction between an Electron Bunch and a Positive Ion Bunch; Dec 1997

NIFS-530 J. Uramoto,
Measuring Method of Decay Time of Negative Muonlike Particle by Beam Collector Applied RF Bias Voltage; Dec. 1997

NIFS-531 J. Uramoto,
Confirmation Method for Metal Plate Penetration of Low Energy Negative Pionlike or Muonlike Particle Beam under Positive Ions; Dec. 1997

NIFS-532 J. Uramoto,
Pair Creations of Negative and Positive Pionlike (Muonlike) Particle or K Mesonlike (Muonlike) Particle in H2 or D2 Gas Discharge in Magnetic Field, Dec. 1997

NIFS-533 S Kawata, C. Boonmee, T. Teramoto, L. Drska, J Limpouch, R. Liska, M. Sinor,
Computer-Assisted Particle-in-Cell Code Development; Dec. 1997

NIFS-534 Y. Matsukawa, T Suda, S. Ohnuki and C. Namba,
Microstructure and Mechanical Property of Neutron Irradiated TiNi Shape Memory Alloy; Jan. 1998

NIFS-535 A. Fujisawa, H. Iguchi, H. Idei, S. Kubo, K. Matsuoka, S. Okamura, K. Tanaka, T. Minami, S. Ohdachi, S. Morita, H. Zushi, S. Lee, M. Osakabe, R Akiyama, Y Yoshimura, K. Toi, H Sanuki, K. Itoh, A. Shimizu, S. Takagi, A. Ejiri, C. Takahashi, M Kojima, S. Hidekuma, K Ida, S. Nishimura, N. Inoue, R. Sakamoto, S.-I. Itoh, Y. Hamada, M. Fujiwara,
Discovery of Electric Pulsation in a Toroidal Helical Plasma, Jan. 1998

NIFS-536 Lj.R. Hadzievski, M.M. Skoric, M. Kono and T. Sato,
Simulation of Weak and Strong Langmuir Collapse Regimes, Jan. 1998

NIFS-537 H Sugama, W. Horton,
Nonlinear Electromagnetic Gyrokinetic Equation for Plasmas with Large Mean Flows, Feb. 1998

NIFS-538 H. Iguchi, T.P. Crowley, A Fujisawa, S. Lee, K. Tanaka, T. Minami, S. Nishimura, K Ida, R. Akiyama, Y. Hamada, H., Idei. M Isobe, M. Kojima, S Kubo, S Morita, S. Ohdachi, S. Okamura, M. Osakabe, K. Matsuoka, C Takahashi and K. Toi,
Space Potential Fluctuations during MHD Activities in the Compact Helical System (CHS); Feb. 1998

NIFS-539 Takashi Yabe and Yan Zhang,
Effect of Ambient Gas on Three-Dimensional Breakup in Coronet Formation Process; Feb. 1998

NIFS-540 H. Nakamura, K. Ikeda and S. Yamaguchi,
Transport Coefficients of InSb in a Strong Magnetic Field; Feb. 1998

NIFS-541 J. Uramoto,
Development of ν_μ Beam Detector and Large Area ν_μ Beam Source by H_2 Gas Discharge (I); Mar. 1998

NIFS-542 J. Uramoto,
Development of $bar\{\nu\}_\mu$ Beam Detector and Large Area $bar\{\nu\}_\mu$ Beam Source by H_2 Gas Discharge (II); Mar. 1998

NIFS-543 J. Uramoto,
Some Problems inside a Mass Analyzer for Pions Extracted from a H_2 Gas Discharge; Mar. 1998

NIFS-544 J. Uramoto,
Simplified ν_μ $bar\{\nu\}_\mu$ Beam Detector and ν_μ $bar\{\nu\}_\mu$ Beam Source by Interaction between an Electron Bunch and a Positive Ion Bunch; Mar. 1998

NIFS-545 J. Uramoto,
Various Neutrino Beams Generated by D_2 Gas Discharge; Mar.1998

NIFS-546 R. Kanno, N. Nakajima, T. Hayashi and M. Okamoto,
Computational Study of Three Dimensional Equilibria with the Bootstrap Current; Mar. 1998

NIFS-547 R. Kanno, N. Nakajima and M. Okamoto,
Electron Heat Transport in a Self-Similar Structure of Magnetic Islands; Apr. 1998

NIFS-548 J.E. Rice,
Simulated Impurity Transport in LHD from MIST; May 1998

NIFS-549 M.M. Skoric, T. Sato, A.M. Maluckov and M.S. Jovanovic,
On Kinetic Complexity in a Three-Wave Interaction; June 1998

NIFS-550 S. Goto and S. Kida,
Passive Saclar Spectrum in Isotropic Turbulence: Prediction by the Lagrangian Direct-interaction Approximation; June 1998

NIFS-551 T. Kuroda, H. Sugama, R. Kanno, M. Okamoto and W. Horton,
Initial Value Problem of the Toroidal Ion Temperature Gradient Mode ; June 1998

NIFS-552 T. Mutoh, R. Kumazawa, T. Seki, F. Simpo, G. Nomura, T. Ido and T. Watari,
Steady State Tests of High Voltage Ceramic Feedthoughs and Co-Axial Transmission Line of ICRF Heating System for the Large Helical Device ; June 1998

NIFS-553 N. Noda, K. Tsuzuki, A. Sagara, N. Inoue, T. Muroga,
oronaization in Future Devices -Protecting Layer against Tritium and Energetic Neutrals-: July 1998

NIFS-554 S. Murakami and H. Saleem,
Electromagnetic Effects on Rippling Instability and Tokamak Edge Fluctuations; July 1998

NIFS-555 H. Nakamura, K. Ikeda and S. Yamaguchi,
Physical Model of Nernst Element; Aug. 1998

NIFS-556 H. Okumura, S. Yamaguchi, H. Nakamura, K. Ikeda and K. Sawada,
Numerical Computation of Thermoelectric and Thermomagnetic Effects; Aug. 1998

NIFS-557 T. Yasuhiko, O. Masaki, T. Katsuyoshi, O. Yoshihide, K. Osamu, A. Eiji, K. Toshikazu, A. Ryuichi and T. Masanobu,
Development of a High-Current Hydrogen-Negative Ion Source for LHD-NBI System; Aug.1998